Effects of heat treatment and high-temperature oxidation on 3D-printed Inconel718 alloy

DOI : 10.36909/jer.17965

B. Anush Raj[1], J T Winowlin Jappes[1], M Adam Khan[1]*, N C Brintha[2] and P M Mashinini[3]

1–Department of Mechanical Engineering & Centre for Surface Engineering, Kalasalingam Academy of Research & Education, Virudhunagar, Tamilnadu, India

2–Department of Computer Science and Engineering & Centre for Surface Engineering, Kalasalingam Academy of Research & Education, Virudhunagar, Tamilnadu, India

3- Department. of Mechanical and Industrial Engineering Technology, University of Johannesburg, Johannesburg, South Africa

* Corresponding Author: adamkhanm@gmail.com

ABSTRACT

In the present paper, Inconel 718 alloy was prepared by direct metal laser sintering. The bare alloy was post-processed through different heat-treatment routes, and the changes in its metallurgical and microstructural properties were investigated. In comparison to the bare alloy, grains in the overlapping region of the heat-treated alloys became refined. The strengthening phase of γ' and γ" precipitations was high in the heat-treated alloys. Furthermore, cyclic oxidation studies were conducted on the bare and heat-treated samples at 1000°C. The variation in mass change per unit area and the corresponding corrosion mechanism were explored. Moreover, the formation mechanism of surface oxides under the influence of each alloying element was discussed. Chromium oxides were mainly formed during oxidation, and the mass change of the heat-treated alloys increased with these oxides. Therefore, an appropriate heat-treatment plan is highly recommended to prevent an alloy from continuous degradation and oxide formation.

Keywords: Additive manufacturing, Oxidation, Mass change, Oxides, IN718.

INTRODUCTION

Nickel-based superalloys are extensively applied in high-temperature components, such as gas turbines, aircraft, nuclear power reactors (Pollock et al., 2006). These materials have high oxidation and corrosion resistance with good mechanical properties at elevated temperatures (Jiang et al., 2016) and manifest multiphase characteristics with γ", γ', γ, and δ phases. The γ" phase precipitates in the form of metastable Ni3Nb in body-centered tetragonal structures. The γ' phase precipitates in the form of (Ni_3 (Al, Ti)) in spherical face-centered cubic structures. The γ phase exists in the form of Ni-Cr-Fe in austenite (Sundararaman et al., 1992 & Chaturvedi et al., 1987). The amount of γ' and γ" precipitations controls the grain size and mechanical properties (tensile strength and creep resistance) of alloys (Devaux et al., 2008). In comparison to conventional manufacturing, additive manufacturing can greatly improve the mechanical properties of IN718 alloy (Trosch et al., 2016).

Nickel-based superalloys prepared by additive manufacturing are widely used in aviation and aerospace applications (Wang et al., 2015). Additive manufacturing can produce complex shapes with great dimensional accuracy and surface finish. In comparison to conventional manufacturing processes, additive manufacturing provides good material efficiency, resource efficiency, part flexibility, and production flexibility (Prakashet al., 2018).

The orientation of IN718 alloy prepared by additive manufacturing and found the same grain structure in both transverse and longitudinal orientations after heat treatments (Farber et al., 2018). The IN718 alloys prepared by the additive manufacturing have anisotropy (Smith et al., 2016). The microstructure of IN718 alloy manufactured by direct metal laser sintering (DMLS) and reported the formation of columnar grains and dendrites in the bare sample (Jinoop et al., 2018). The hardness of the AM processed IN718 is mainly depends on the heat treatment process. The annealing above the 1200˚C may decrease the hardness of the alloy (Ciftci et. al., 2021). The surface quality of the IN718 processed by AM is mainly affected by the parameter such as scan speed and power density. At low power density the un-melted

regions where found which reduce the surface quality and mechanical properties of the alloy. Also, with the increase in energy density the thermal strains and key hole effect were occurred which reduce the mechanical characteristics of the alloy. Therefore, the moderate energy density and low scan speed is used to produce quality products (Kladovasilakis et. al., 2022). The mass change due to oxidation and oxide layer thickness of the nickel alloy increased with the rising temperature. Chromium and titanium oxides were formed as protective layers to resist the nickel base from oxidation. Titanium oxides were not found at temperatures above 900°C, resulting in an increase in chromium diffusion (Yun et al., 2017). The oxidation and hot corrosion behavior of a nickel alloy and reported that the cumulative mass change of the alloy in the salt environment was 10–20 times greater than that in the air (Khan et al., 2014). The oxidation behavior of a nickel alloy by isothermal oxidation testing for nickel alloy leads to the formation of Cr_2O_3, TiO_3, and a small amount of $NiCr_2O_4$ in the alloy (Liu et al., 2007). The temperatures above 900°C, internal oxidation occurred in the nickel alloy. When the exposure time increased from five hours to ten hours, the formation of Cr_2O_3 and $NiCr_2O_4$ oxides provided the oxidation resistance for the nickel alloy (El-Awadi et al., 2016). The oxidation mechanism of a nickel-based alloy and found that oxides were mainly formed on grain boundaries and dense spinels acted as protective layers to protect the alloy from oxidation and hot corrosion (Chellaganesh et al., 2018). The diffusion of oxygen started from grain boundaries. Thus oxide formation took place at grain boundaries (Clarke, 2002). Due to temperature drop, stress and strain acted on oxides formed in the nickel alloy, causing the spallation of oxides (Evans et al., 1984). The spallation of oxides can be described as a function of time and temperature and may occur during cooling (Tomlinson et al., 1977).

IN718 alloy prepared by additive manufacturing is extensively used in high-temperature gas turbine applications. The oxidation of IN718 generally initiates at grain boundaries. Homogenization, solutionizing, and aging are generally applied to refine grain boundaries in IN718 alloy.

Therefore, in the present work, the effects of three different heat-treatment routes on the microstructure and oxidation behavior at 1000°C of IN718 alloy prepared by DMLS were investigated.

EXPERIMENTAL PROCEDURE

Inconel 718 alloy was prepared by direct metal laser sintering (DMLS). A basic sketch of the proposed DMLS process is displayed in Figure 1. The metal powder was spread over the building bed of a powder feeding system by a scoop. The metal powder was fused over the bed by a laser. The process was continued until the required sample dimension was obtained. The alloy was developed layer by layer in an isentropic form. The chemical composition of the material used for DMLS is presented in Table 1. The IN718 powder was gas atomized and manufactured in an EOS M280 DMLS machine under the optimum processing parameters of power = 285W, scan rate = 970 mm/s, hatching distance = 0.15 mm, layer thickness = 40 µm, and beam diameter = 80 µm. The samples were built in horizontal orientation with a size of 15 mm x 15 mm x 6 mm. The employed heat-treatment plans for the samples are presented in Table 2, and the order of different heat-treatment cycles is displayed in Figure 2. After heat treatments, the samples were cleaned and polished with emery papers of up to 2000 grid size. Each sample was placed in an alumina crucible separately, and their initial weights were measured in an electronic balance. Cyclic oxidation studies were carried out in a tubular furnace at 1000°C and 85% humidity in the air. The experiment was carried out for 20 cycles with a holding time of 5 hr to complete 100 hr. The mass change of the air-cooled samples was calibrated for every cycle.

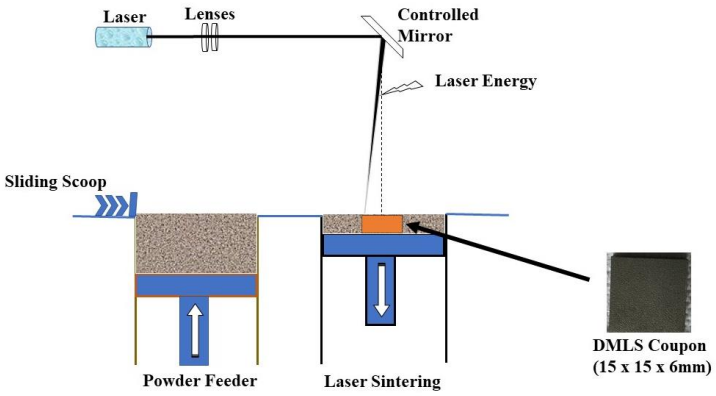

Figure 1. Basic sketch of direct metal laser sintering

Table 1. Elemental Composition

Element	Ni	Fe	Cr	Nb	Mo	Ti	Al	Si	C	Co	Cu	W
Weight%	52.44	19.78	17.13	4.77	3.38	1.11	0.59	0.13	0.05	0.16	0.23	0.23

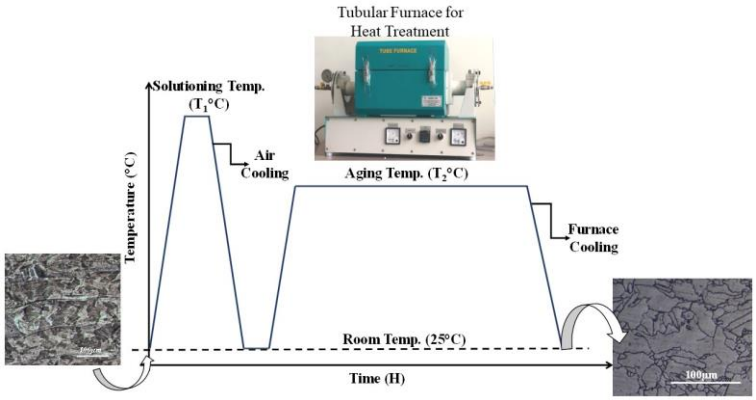

Figure 2. Order of different heat-treatment (HT) cycles

Table 2. Heat-treatment Regimes

Plan	Solutionizing/Annealing (T1)			Ageing (T2)		
	Temp (°C)	Time (H)	Cooling	Temp (°C)	Time (H)	Cooling
HT 1	980 °C	1 Hour	Air	720 °C	8 Hours	Furnace cooled at 55°C/h
				620 °C	8 Hours	Furnace cooled at 55°C/h
HT 2	1100 °C	2 Hours	Air	845 °C	24 Hours	Furnace cooled at 55°C/h
HT 3	1100 °C	2 Hours	Air	845°C	12 Hours	Furnace cooled at 55°C/h

The microstructure and crystal structure of the heat-treated and bare samples after etching

were characterized by an optical microscope and an X-ray diffractometer (Bruker ECO D8 Advance), respectively. The composition of oxides formed on the exposed samples was analyzed by a scanning electron microscope (Zeiss–FE SEM) attached to an energy-dispersive X-ray diffractometer (EDX).

RESULTS AND DISCUSSION

Microstructure on the heat-treated DMLS alloys

DMLS is a layer by layer manufacturing process, and the texture of the as-built sample is displayed in Figure 3a. The bonding of the metal in the form of layers was tracked throughout the sample. The metal pool was built in the vertical direction, and the scanning was performed in the horizontal direction. An overlapping layer region of metal binding was noticed in the microstructure. In this overlapping region, the formation of dendrites was detected.

The microstructure of the HT1 DMLS IN718 alloy is presented in Figure 3b. In this sample, grains were elongated and not completely homogenized. The grains are refined within the scan track itself and metal pool arc are clearly noticed for HT1 alloy. Similar to the bare alloy, refined grains and columnar dendrites were found in the HT1 alloy. The precipitation of the gamma phase took place at low temperatures in a short period (Jambor et al., 2017). The microstructures of the HT2 alloy is shown in figure 3c. The grains are fine and fully homogenized takes place on the overlap region. Some large grains are found on the HT2 alloys which are in columnar structure. Also, for HT2 alloy the metal pool arc is fully disappeared and recrystallization structure takes place. The figure 3d represents the microstructure of HT3 alloy. In HT3 alloy at the overlap region the fine grains are formed and within the layer the elongated columnar grains are formed. The alloy is heated above 1100˚C the metal arc boundaries where disappeared.

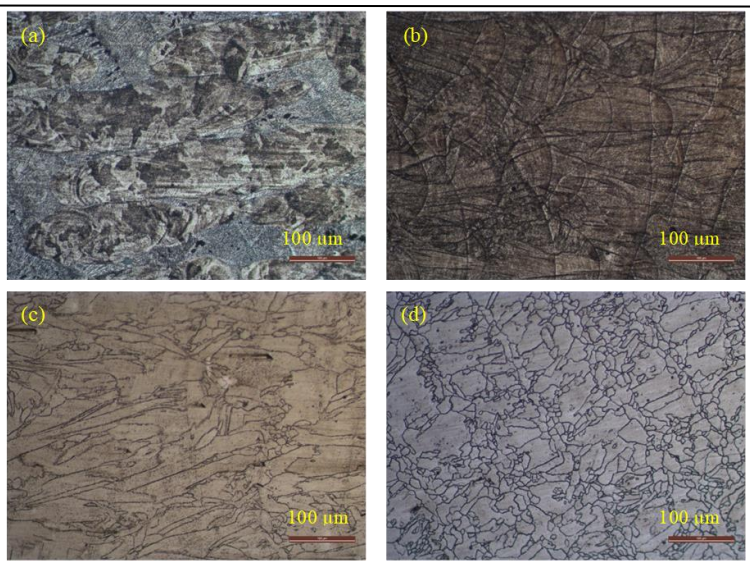

Figure 3. Microstructure of the (a) bare, (b) HT1, (c) HT2, (d) HT3 DMLS IN718 alloys

Oxidation behavior of the DMLS alloys

The oxidation kinetics of IN718 was studied. The calculated mass change rates per unit area ($\Delta mg/cm^2$) during high-temperature oxidation at 1000°C are displayed in Figure 4. The first 30 h of oxidation was the incubation period because the mass change was very gradual in all the heat-treated and bare alloys. In this period, as the bare alloy underwent sintering and homogenization, it exhibited lower mass change as compared to the heat-treated alloys. After the incubation period, the mass change of the HT1 and HT2 alloys was between 0.3–0.5 mg/cm^2; therefore, their mass change was stable. The mass change of the bare alloy after the incubation period was catastrophic, and after 50 h, the mass change became stable. The mass change of the HT3 alloy was vulnerable as compared to the other alloys. At the end of 100 h, the minimum mass change was found in the HT1 and HT2 alloys, whereas the maximum mass change was detected in the HT3 DMLS alloy.

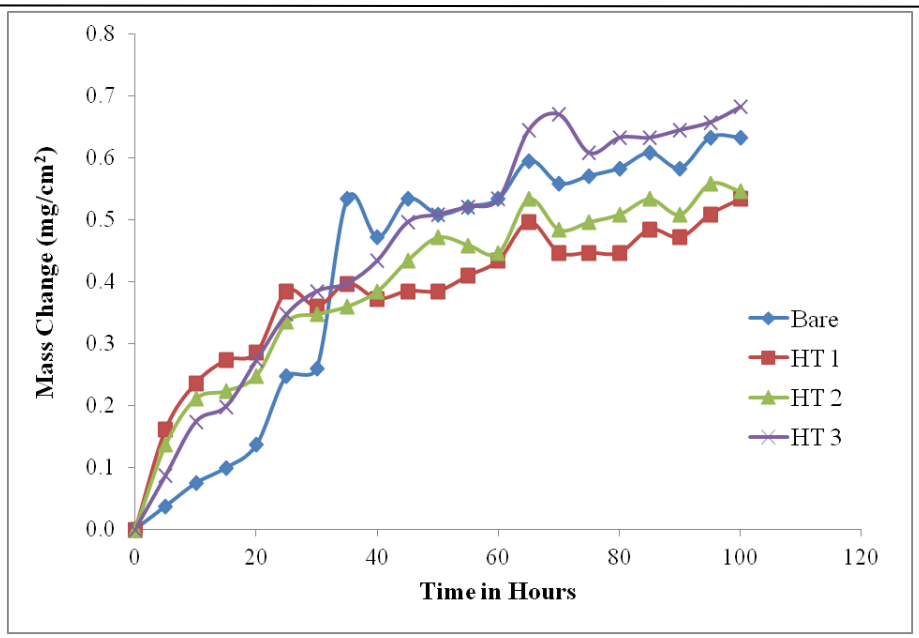

Figure 4. Mass change during cyclic oxidation at 1000°C

Surface topology

The samples exposed in the air for 100 h were masked by dark grey scales without spallation. The surface morphologies of the bare and heat-treated samples are displayed in Figure 5. Globular oxide scales were formed on the high-temperature oxidized samples. Oxides formed on the bare and HT3 alloys were denser than those formed on the HT1 and HT2 samples. The wrinkling of oxides was observed in all oxidized samples due to the growth of lateral oxides. In the bare sample, porous oxides were formed. In addition to porous oxides, some nodular oxides were also formed in the HT1 oxidized sample. The porous oxides and oxides formed on the overlap region is high for the bare DMLS alloy which is shown in figure 5a, which leads to high mass change in the alloy when compared to HT1 and HT2 alloys. The HT3 alloy also found very fine grains in the overlap region which leads to the increase in the grain boundaries. The oxidation nucleation starts in the grain boundaries. Therefore, the mass change is very high for the HT3 alloy which is clearly identified in the form dense of globular oxides in the figure 5d. These swelling of oxides formed in the grain boundaries of the alloys improve the oxidation scale faster. The similar results of globular oxides and swelling of oxides in the grain boundaries of the AM processed IN718 alloy found in the literature

(Sanviemvongsak et. al., 2018).

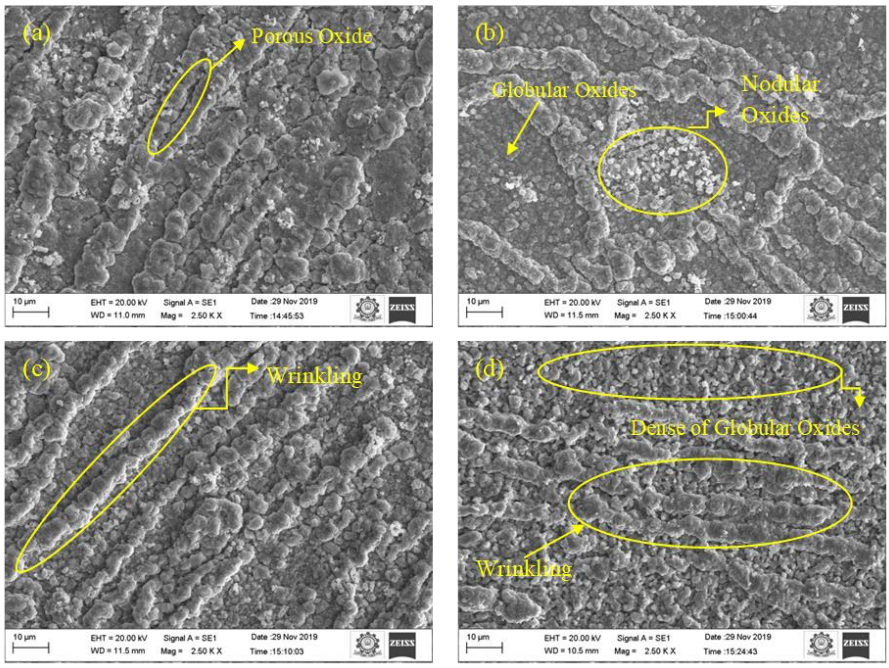

Figure 5. Microstructures of the oxidized (a) bare, (b) HT1, (c) HT2, (d) HT3 DMLS IN718 alloys

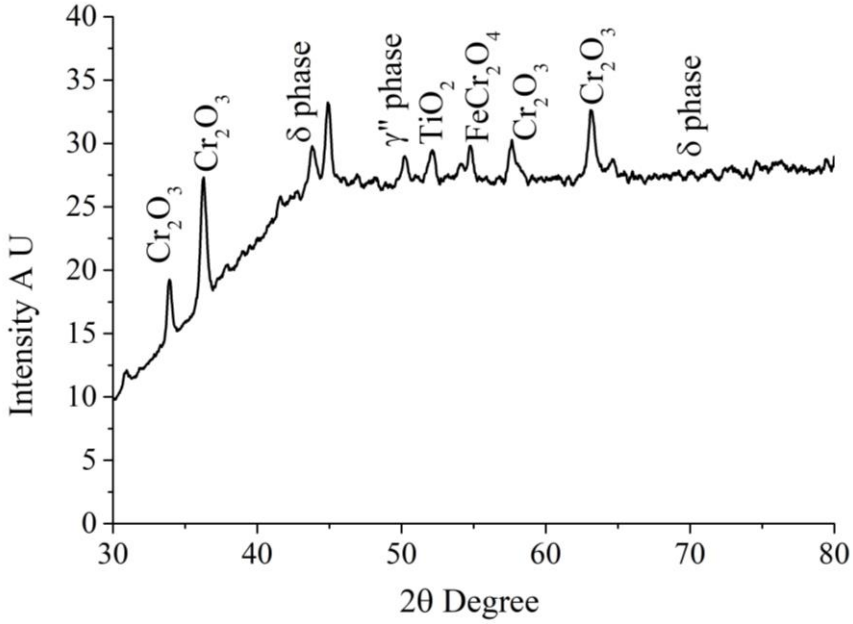

Figure 6. XRD of oxidized DMLS bare sample

The XRD analysis was performed for the oxidized DMLS bare sample is shown in figure 6. It was found that the chromium oxides are found in rich and some traces of iron chromium

oxide and titanium oxides.

EDX analysis

The EDX spectra of the oxidized bare, HT1, HT2, and HT3 DMLS alloys during oxidation are displayed in Figures 7–10, respectively. The EDX analysis of DMLS oxidized alloy clearly denotes that chromium and oxygen elements are rich. The oxidation studies of IN718 on literature reported that the Cr_2O_3 scale was formed on the grain boundaries and $NiCr_2O_4$ and Fe_2O_3 mixed scale is formed on the surface of the IN718 alloy (Juillet et. al., 2018). The existence of Cr, O, Ni, Nb, Si, Fe, and Ti was detected in the DMLS samples; however, the contents of chromium and oxygen were found to be relatively higher. Therefore, the samples were mainly protected by chromium oxides, and the mass change of the heat-treated alloys increased with these oxides. The percentages of chromium and oxygen precipitation in the bare, HT1, HT2, and HT3 alloys were 90%, 88%, 88%, and 91%, respectively.

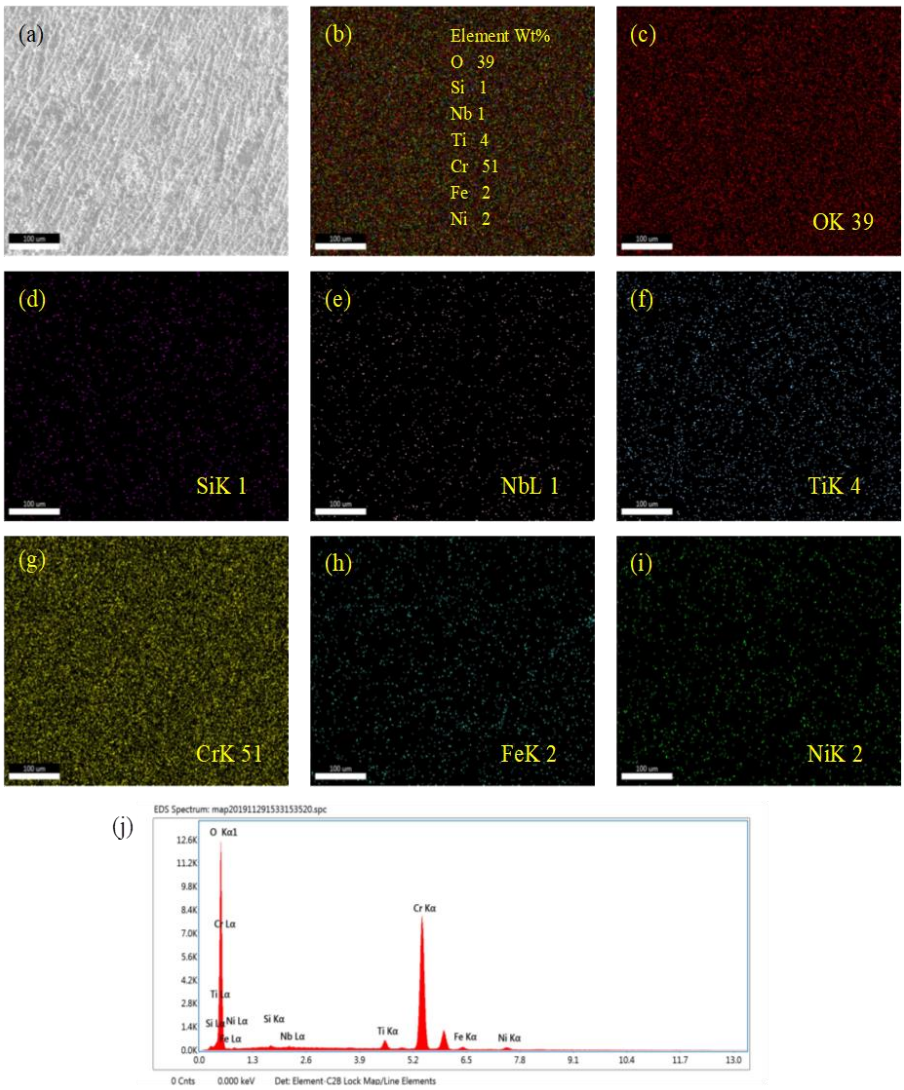

Figure 7. EDX spectra of the bare DMLS alloy

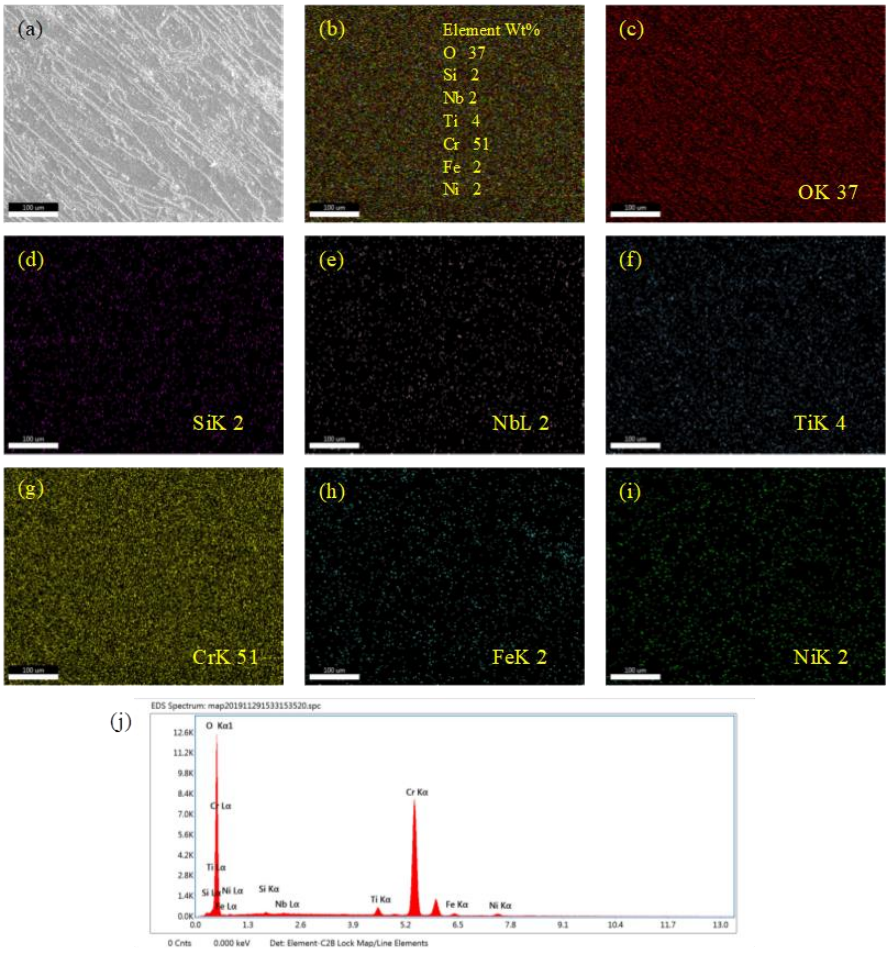

Figure 8. EDX spectra of the HT1 DMLS alloy

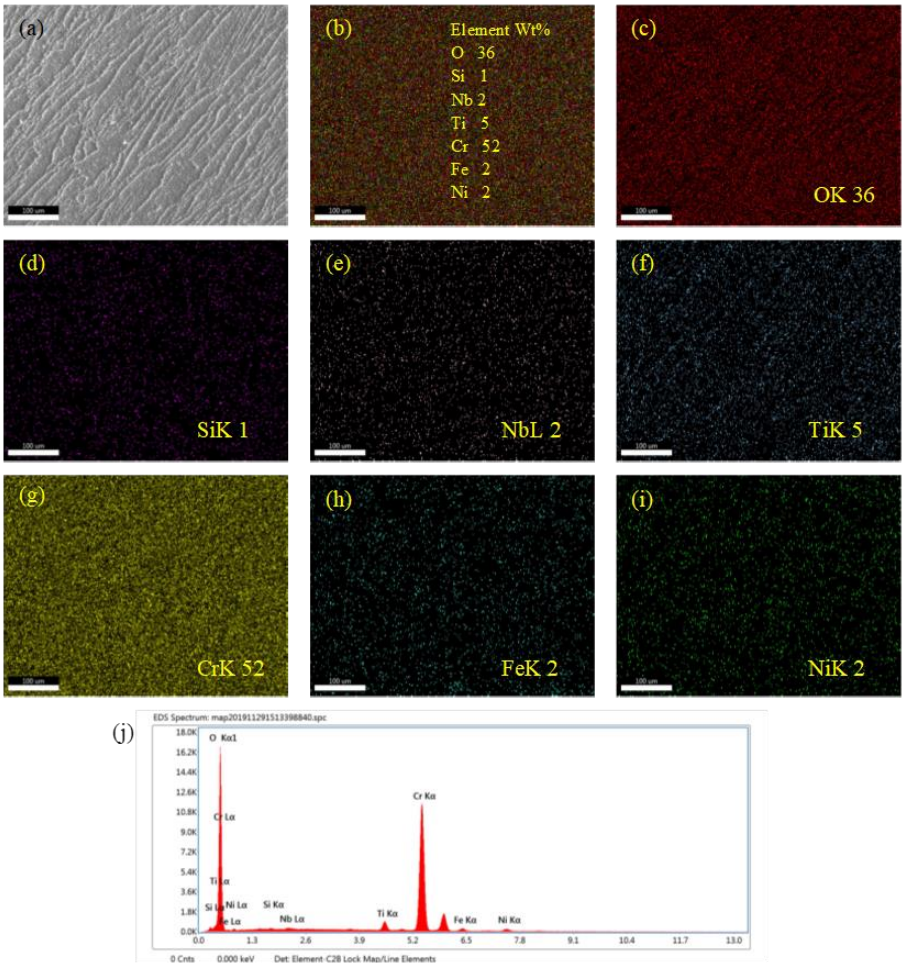

Figure 9. EDX spectra of the HT2 DMLS alloy

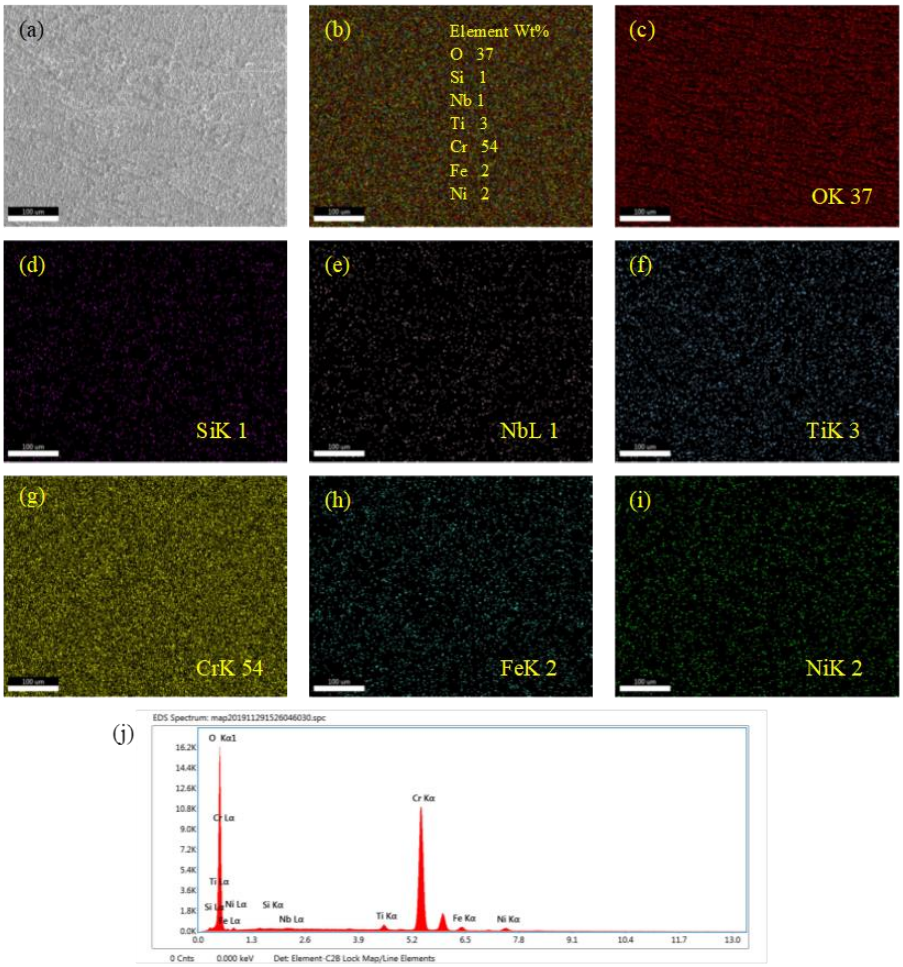

Figure 10. EDX spectra of the HT3 DMLS alloy

CONCLUSION

In the present study, the effects of heat treatment on the microstructure and oxidation behavior of IN718 superalloy manufactured by DMLS were investigated. The main observations are presented below.

1. After heat treatments, grains were refined in each metal pool of HT1, and full homogenization took place in the HT2 and HT3 alloys.

2. The minimum mass change was detected for the HT1 and HT2 alloys; thus, these alloys experienced lower oxide formation as compared to the bare and HT3 DMLS alloys.

3. The oxide formation starts on the grain boundary of the alloy. The porous oxides formed on the bare alloy and nodular and globular oxides are formed on the heat treated sample.

4. Chromium oxides were mainly formed during oxidation, and the mass change of the heat-treated alloys increased with these oxides.

REFERENCES

Pollock, T. M., & Tin, S. 2006. Nickel-based superalloys for advanced turbine engines: chemistry, microstructure and properties. Journal of propulsion and power, 22(2), 361-374.

Jiang, R., & Reed, P. A. S. 2016. Critical Assessment 21: oxygen-assisted fatigue crack propagation in turbine disc superalloys. Materials Science and Technology, 32(5), 401-406.

Sundararaman, M., Mukhopadhyay, P., & Banerjee, S. 1992. Some aspects of the precipitation of metastable intermetallic phases in INCONEL 718. Metallurgical Transactions A, 23(7), 2015-2028.

Chaturvedi, M. C., & Han, Y. 1987. Effect of particle size on the creep rate of superalloy Inconel 718. Materials Science and Engineering, 89, L7-L10.

Devaux, A., Nazé, L., Molins, R., Pineau, A., Organista, A., Guédou, J. Y., & Héritier, P. 2008. Gamma double prime precipitation kinetic in Alloy 718. Materials Science and

Engineering: A, 486(1-2), 117-122.

Trosch, T., Strößner, J., Völkl, R., & Glatzel, U. 2016. Microstructure and mechanical properties of selective laser melted Inconel 718 compared to forging and casting. Materials letters, 164, 428-431.

Wang, X., Gong, X., & Chou, K. 2015. Review on powder-bed laser additive manufacturing of Inconel 718 parts. In International Manufacturing Science and Engineering Conference (Vol. 56826, p. V001T02A063). American Society of Mechanical Engineers.

Prakash, K. S., Nancharaih, T., & Rao, V. S. 2018. Additive manufacturing techniques in manufacturing-an overview. Materials Today: Proceedings, 5(2), 3873-3882.

Farber, B., Small, K. A., Allen, C., Causton, R. J., Nichols, A., Simbolick, J., & Taheri, M. L. 2018. Correlation of mechanical properties to microstructure in Inconel 718 fabricated by direct metal laser sintering. Materials Science and Engineering: A, 712, 539-547.

Smith, D. H., Bicknell, J., Jorgensen, L., Patterson, B. M., Cordes, N. L., Tsukrov, I., & Knezevic, M. 2016. Microstructure and mechanical behavior of direct metal laser sintered Inconel alloy 718. Materials Characterization, 113, 1-9.

Jinoop, A. N., Subbu, S. K., & Kumar, R. A. 2018. Mechanical and microstructural characterisation on direct metal laser sintered Inconel 718. International Journal of Additive and Subtractive Materials Manufacturing, 2(1), 1-12.

Ciftci, J., Sitek, R., & Mizera, J. (2021). Analysis of direct metal laser sintering–DMLS and heat treatment influence on the Inconel 713C nickel alloy structure. Welding Technology Review, 93.

Kladovasilakis, N., Charalampous, P., Tsongas, K., Kostavelis, I., Tzovaras, D., & Tzetzis, D. (2022). Influence of Selective Laser Melting Additive Manufacturing Parameters in Inconel 718 Superalloy. Materials, 15(4), 1362.

Yun, J. Y., Park, D., & Wang, J. P. 2017. A study on the oxidation behavior of nickel alloys at elevated temperatures. In IOP Conference Series: Materials Science and Engineering (Vol. 191, No. 1, p. 012039). IOP Publishing.

Khan, M. A., Sundarrajan, S., Natarajan, S., Parameswaran, P., & Mohandas, E. 2014. Oxidation and hot corrosion behavior of nickel-based superalloy for gas turbine applications. Materials and manufacturing processes, 29(7), 832-839.

Liu, F. J., Zhang, M. C., Dong, J. X., & Zhang, Y. W. 2007. High-temperature oxidation of FGH96 P/M superalloy. Acta Metallurgica Sinica (English Letters), 20(2), 102-110.

El-Awadi, G. A., Abdel-Samad, S., & Elshazly, E. S. 2016. Hot corrosion behavior of Ni based Inconel 617 and Inconel 738 superalloys. Applied surface science, 378, 224-230.

Chellaganesh, D., Khan, M. A., Jappes, J. W., & Sathiyanarayanan, S. 2018. Cyclic oxidation and hot corrosion behavior of nickel–iron-based superalloy. High Temperature Materials and Processes, 37(2), 173-180.

Clarke, D. R. 2002. Stress generation during high-temperature oxidation of metallic alloys. Current opinion in solid state and materials science, 6(3), 237-244.

Evans, H. E., & Lobb, R. C. 1984. Conditions for the initiation of oxide-scale cracking and spallation. Corrosion Science, 24(3), 209-222.

Tomlinson, W. J., Gardner, M. J., & Kowalski, R. J. 1977. The scale constituents and spalling characteristics of Ni-Fe (0–60%) alloys oxidized in air at 800–1200° C. Corrosion Science, 17(4), 301-304.

Jambor, M., Bokuvka, O., Novy, F., Trsko, L., & Belan, J. 2017. Phase transformations in nickel base superalloy inconel 718 during cyclic loading at high temperature. Production engineering archives, 15.

Sanviemvongsak, T., Monceau, D., & Macquaire, B. (2018). High temperature oxidation of IN 718 manufactured by laser beam melting and electron beam melting: Effect of surface

topography. Corrosion Science, 141, 127-145.

Juillet, C., A. Oudriss, J. Balmain, X. Feaugas, and F. Pedraza. (2018) "Characterization and oxidation resistance of additive manufactured and forged IN718 Ni-based superalloys." Corrosion Science 142 (2018): 266-276.